Photoionization of atomic iodine and atomic tellurium

J. Berkowitz, C. H. Batson, and G. L. Goodman
Physics Division, Argonne National Laboratory, Argonne, Illinois 60439
(Received 13 January 1981)

Mass-analyzed photoionization spectra have been obtained from beams of atomic iodine and atomic tellurium from their respective ionization thresholds to ~19 eV. In each instance the ionization thresholds are confirmed. For iodine, most of the features in the autoionization resonance spectrum have been identified and assigned to several s- and d-like Rydberg series converging to the higher-ionization limits $^3P_0$, $^3P_1$, $^1D_2$, and $^1S_0$ of the $5s^25p^4$ configuration. For tellurium we also observe autoionization resonance features assigned to s- and d-like Rydberg series converging to the higher-ionization limits $^2D_{3/2}$, $^2D_{5/2}$, $^2P_{1/2}$, and $^2P_{3/2}$ of the $5s^25p^3$ configuration. In addition, a window-resonance series and additional peaks have been assigned as converging to the $5s5p^4\,^4P_{5/2}$ state of Te^+, with quantum defect of ~0.5 (modulo 1). In both elements, the d-like series exhibits anomalous resonance profiles similar to those in the heavier noble gases, with quantum defects of ~0.4 (modulo 1). The s-like series has quantum defects of ~0.0 (modulo 1). Some comparisons are made with many-body calculations on the related chlorine atom.

I. INTRODUCTION

The photoionization of atoms has received increasing attention from both experimentalists and theoreticians in the past 10–15 years. The experiments have been directed toward the determination of total and partial cross sections as a function of wavelength, the measurement of angular distributions and spin polarizations of the ejected photoelectrons, and the observation of autoionizing resonances. The calculations, initially employing independent-particle wave functions (Herman-Skillman and later Hartree-Fock) for bound and continuum states,[1] have become more sophisticated in order to explain quantitatively the experimental observations. These latter calculations are described as RPAE (random-phase approximation with exchange),[2] diagrammatic many-body theory,[3] R-matrix formalism,[4] and more recently, relativistic versions of these methods.[5-7] Perhaps the most successful of these calculational techniques to date has been the relativistic random-phase approximation, which is used to obtain the parameters for multichannel quantum-defect theory. Recently, Johnson and collaborators have used this scheme to calculate angular distribution and spin polarization of photoelectrons and the energies and profiles of resonances in the noble gases Ne, Ar, Kr, and Xe, in very good agreement with experiment.

However, this method has not yet been applied to open-shell atoms. Manson *et al.*[8] note that "... approximately 75% of the elements of the periodic table are unstudied experimentally," and most of these are open-shell atoms. In this context, two interesting test groups for study are the halogens ($...np^5$) and chalcogens ($...np^4$). Manson *et al.*[8] have recently reported calculations at the Herman-Skillman and Hartree-Fock level for both these classes of atoms. These calculations are insensitive to the presence of resonances; they have focused on total and partial cross sections and angular distributions of photoelectrons from direct ionization to the continuum. The partial cross sections are not in good agreement with recent photoelectron data on atomic Cl (Ref. 9), Br (Ref. 9), and I (Ref. 10). By contrast, a relatively simple angular momentun coupling scheme[10] yields these branching ratios in very good agreement with experiment.

Recently, the energies and profiles of the autoionizing resonances in Cl have been calculated by Lamoureaux and Combet-Farnoux[11] using the R-matrix formalism, and by Brown *et al.*[12] using many-body perturbation theory. Also of relevance are the calculations of McGuire[13] on autoionization of the chalcogen atoms. He was interested in possible laser action for these atoms involving the excited $^1S_0$ state, and hence computed a possible loss mechanism in which this excited state was autoionized. His calculations were primarily at the Herman-Skillman level.

In previous photoelectron studies, we had found that the volatilization of AgI produced a clean source of atomic iodine in its ground state, which could be used for wavelength-dependent photoionization experiments. We also sought to extend both photoelectron and photoion experiments to the chalcogens, and toward this end we found a suitable source for atomic tellurium, for which we also obtained photoionization-yield data.

II. EXPERIMENTAL ARRANGEMENT

An atomic iodine beam was obtained, as before, by vaporizing AgI from a tungsten crucible which was heated by radiation from a resistively heated tungsten spiral. This oven design has been de-

scribed previously.[14] The vaporization temperature is around 950–1000 K. The atomic beam is crossed by a photon beam which has been previously dispersed by a 3-meter, normal-incidence monochromator. The hydrogen many-lined emission spectrum and the Hopfield continuum of helium served as light sources over the experimental region of ~650 Å to ionization threshold. The wavelength resolution was 0.28 Å full width at half maximum. Impurity lines in the light source served as wavelength calibrants in the Hopfield continuum region. The many-lined hydrogen molecular emission spectrum was initially calibrated by generating the argon resonance lines at 1048 and 1066 Å as primary calibrants, and then stepping through the hydrogen emission region. The hydrogen wavelengths were then compared with the atlas of hydrogen lines reported by Schubert and Hudson.[15] Identified features agreed to within 0.2 Å. The identified hydrogen wavelengths were then slightly shifted to provide improved agreement with Schubert and Hudson, generally to ±0.05 Å and no worse than 0.1 Å. Photoions generated were drawn out and focused by an ion-lens system into a quadrupole mass spectrometer. The mass-selected ions were measured and the wavelength (as determined by a shaft encoder) recorded. Since counting rates were low, it was essential to maintain a low background (a few counts per minute). Long counting times (between 10 and 60 sec/point) were required. The AgI sample had the unpleasant feature of changing its vaporization rate with time. Corrections were made for this behavior by making rapid point scans over extended wavelength ranges, and normalizing our point-by-point data to these rapid-scan results.

The vapor above AgI contained a significant abundance of AgI and I_2, as well as I. It almost certainly contained Ag_3I_3 as well, although our mass analyzer was unable to probe this high mass. The experimental evidence does not indicate any contribution from these additional species between threshold and ~1000 Å, and probably also to the limit of the experimental data. The adiabatic ionization potential af AgI was measured in a separate experiment.

With the chalcogen series, interest rapidly focused on tellurium because sulfur and selenium tend to form complex molecular species. Elemental tellurium vaporizes at ~700 K, the vapor consisting largely of Te_2. Thermochemical calculations indicate that a temperature of ~1300 K is necessary at the experimental pressure to produce significant atomic species. This is difficult to achieve by double-oven experiments. A search was made for compounds whose decomposition pressure was in the right range to drive the equilibrium towards the atomic species. Ag_2Te was initially used, and provided an adequate source of Te ($T \cong 1350$ K) for the wavelength region ~1070 Å to threshold. However, the Te_2: Te ratio was about 6 : 1, which meant that the process

$$Te_2 + h\nu \rightarrow Te^+ + Te + e$$

could contribute to the Te^+ signal at photon energies above the thermochemical threshold. The compound Cu_2Te proved more generally useful, since the Te_2:Te ratio observed here was ~1.2 : 1, and this sample was utilized for the bulk of the measurements.

In these latter measurements, at about 1400 K, background ions were detected emanating directly from the oven, perhaps by surface ionization. This unwanted background was suppressed by installing deflector plates between the oven and ionization chamber. The evolution of Te vapor was smoother than in the corresponding AgI experiments.

III. EXPERIMENTAL RESULTS

A. Atomic iodine

The photoionization process represented symbolically by

$$p^5 + h\nu \rightarrow p^4 + e$$

should give rise to 5 ionic states. These states, and their onset wavelengths for iodine, according to Huffman *et al.*[16] are $^3P_2$, 1186.32 Å; $^3P_0$, 1102.02 Å; $^3P_1$, 1094.32 Å; $^1D_2$, 1020.79 Å and $^1S_0$, 878.77 Å. The photoionization spectrum of iodine obtained by us in this wavelength domain is shown in Fig. 1. The $^3P_2$ threshold can be seen as a truncated shoulder of an autoionization peak at the ionization threshold. Our threshold is slightly (~1 Å) lower than that given by Huffman *et al.*[16] The wavelengths in both experiments have been calibrated against standards to within 0.1 Å. Huffman *et al.* have observed Rydberg series up to $n^* = 25.1$ converging to the $^3P_2$ threshold, with rather constant quantum defect corresponding to their limit. Hence, our lower threshold is most likely due to a combination of electric field and collisional ionization of high Rydberg states.

In the tellurium experiment (*vide infra*) the ionization threshold observed agreed with literature values, within experimental error. Since the electric fields (repeller, draw-out) employed in both iodine and tellurium experiments were similar, the more likely cause of the lowered threshold for I^+ is collisional ionization. Iodine atoms generated in our oven source recombine in the ionization chamber, giving rise to a substant-

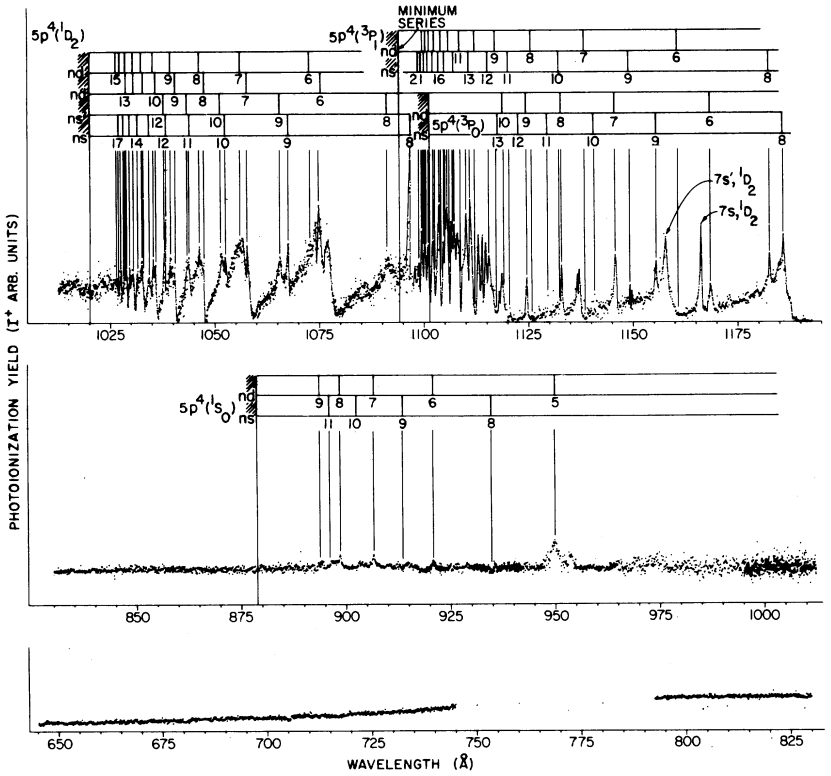

FIG. 1. Relative yield of I^+ in the photoionization process $I(^2P_{3/2})+h\nu \rightarrow I^+ + e$. Identified Rydberg series and their convergence limits are indicated. The running Rydberg indices are chosen to correspond to the convention adopted by Moore (Ref. 19), i.e., $n \simeq n^* + 4$ (ns series) and $n \simeq n^* + 1.5$ (nd series).

ial I_2 pressure. The I_2 molecules are the presumed partners in collisional ionization of I**. In the tellurium experiment, recombination would produce the relatively involatile Te_2.

In order to provide a framework for discussing the resonant structure, let us consider the allowed Rydberg series for this atom. A $5p$ electron can be excited to $ns_{1/2}$, $nd_{3/2}$, and $nd_{5/2}$ Rydberg orbitals. When combined with a $J=0$ core (corresponding to $^1S_0$ or $^3P_0$) this yields $J=\frac{1}{2}$, $\frac{3}{2}$, and $\frac{5}{2}$ composite upper states. If we have a $J=2$ core (corresponding to $^1D_2$ or $^3P_2$) the composite states which are permitted by electric dipole transitions are $J=\frac{3}{2}$ and $\frac{5}{2}$ for Rydberg s orbitals and $J=\frac{1}{2}$, $\frac{3}{2}$, $\frac{5}{2}$ for Rydberg d orbitals. There are also forbidden $J=\frac{7}{2}$ and $\frac{9}{2}$ composite states for the latter. The $^3P_1$ core also yields composite states having $J=\frac{1}{2}$ and $\frac{3}{2}$ for Rydberg s orbitals and $J=\frac{1}{2}$, $\frac{3}{2}$, $\frac{5}{2}$ composite states for Rydberg d orbitals, with a forbidden $\frac{7}{2}$ composite state for the latter.

In Fig. 1, we have identified broad, intense Rydberg members of 2 series having anomalous resonance profiles ($q \approx 1$ in Fano's terminology)[17] whose minima have virtually zero cross section, with a quantum defect of about 0.3, which converge to the $^1D_2$ state. These are presumably 2 of the Rydberg d-like series expected. In addition, there are 2 series of very sharp peaks, having a quantum defect of ~0, also converging to $^1D_2$, which we identify with the anticipated Rydberg s-like series.

We are able to distinguish 2 series converging to $^3P_0$, both rather weak. One, tentatively assigned as an ns series, has quantum defects averaging 0.9; the other, tentatively assigned as an nd series, has quantum defects averaging 0.3. For the $^3P_1$ convergence limit, we have identified 2 series, both becoming more prominent and distinguishable in their higher members. A series assigned as ns has quantum defect ~0; the other, assigned as nd, has an average quantum defect ~0.5. Two series are also discernible which converge to $^1S_0$; an ns series with quantum defect ~0.95 and an nd series with quantum defect ~0.4.

We have only indicated a few points in the region between 745 and 793 Å. This region was examined several times, and some weak features were observed but were not reproducible from one run to the next. Irregular evolution of vapor and a variable ratio of atomic to molecular iodine was suspected. In particular, no evidence of window resonances was observed during these scans.

The wavelengths of identified features in these series, together with their effective quantum numbers are listed in Table I. A separate list of unidentified lines is also included.

B. Atomic tellurium

For the photoionization process

$$p^4 + h\nu \rightarrow p^3 + e\,,$$

we again anticipate 5 final ionic states. In the case of tellurium, we are unaware of any previous work, photoabsorption or photoionization in the relevant wavelength region. However, by resorting to Eriksson's[18] energy levels for TeII and Moore's[19] ionization potential for TeI, we can predict the following threshold wavelengths: $^4S_{3/2}$, 1376.14 Å; $^2D_{3/2}$, 1206.42 Å, $^2D_{5/2}$, 1175.24 Å; $^2P_{1/2}$, 1072.80 Å, and $^2P_{3/2}$, 1034.14 Å. Our photoionization spectrum of atomic tellurium is displayed in Fig. 2. A weak onset can be observed in the figure at 1376 Å, in agreement with Moore's value for the ionization potential. The allowed Rydberg excitations can be read from Table II.

The most easily distinguishable features in the spectrum are the series members with prominent minima converging to 1175.24 Å, the limit for $^2D_{5/2}$. These minima can be followed to $n^* = 14.6$, and are almost certainly a Rydberg d-like series. A prominent series of maxima and minima with approximately the same quantum defect, can also be observed converging to the $^2D_{3/2}$ limit. Both of these limits agree well with those derived from Eriksson's[18] and Moore's values.[19] There is at least one other series discernible converging to $^2D_{5/2}$, and also one converging to $^2D_{3/2}$, both with quantum defects near zero and hence presumable ns series. In addition, we can assign another nd series converging to $^2D_{3/2}$.

We can identify early members of 3 series converging to $^2P_{3/2}$, one ns and two nd (as judged by their quantum defects), but only a weak ill-defined series with quantum defect ~0.4 can be related to the $^2P_{1/2}$ threshold. At shorter wavelengths, two new types of features appear—at least two intense peaks (at 1038.44 and 1060.46 Å) just before the $^2P_{3/2}$ threshold, and a series of window resonances, with nearby weaker peaks, converging to a

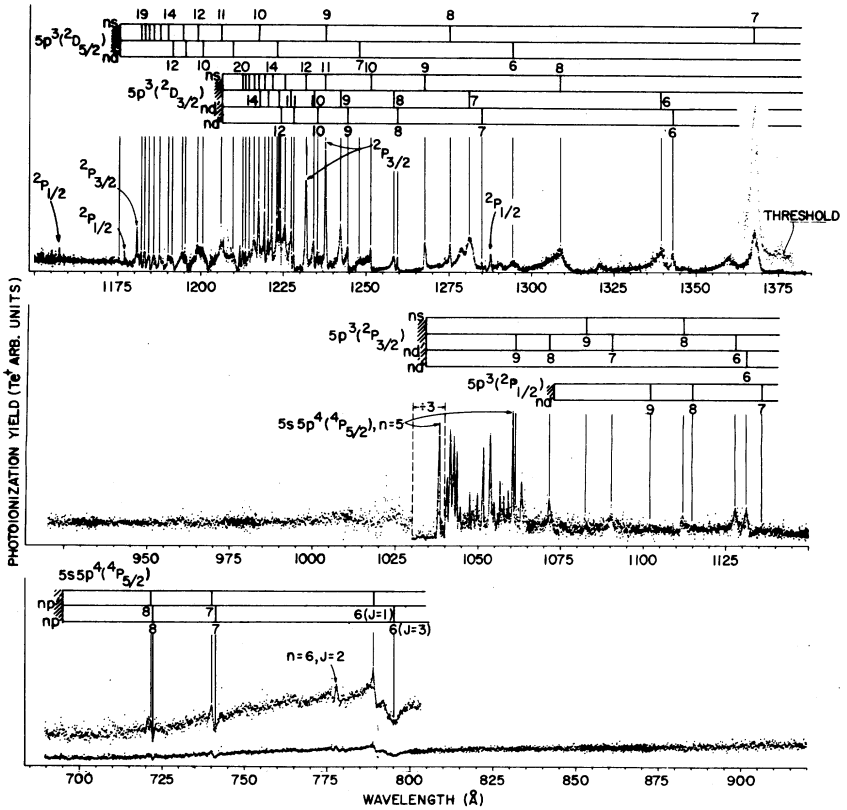

FIG. 2. Relative yield of Te^+ in the photoionization process $Te(^3P_2) + h\nu \rightarrow Te^+ + e$. Identified Rydberg series and their convergence limits are indicated. The running Rydberg indices are chosen to correspond to the convention adopted by Moore (Ref. 19), i. e., $n \simeq n^* + 4$ (ns series) and $n \simeq n^* + 2.5$ (nd series). For the $5s5p^4np$ series, $n \simeq n^* + 3.5$, conforming to the calculations of Cheng and Kim (Ref. 22).

TABLE I. Wavelengths of identified features in Rydberg series, converging to $^3P_0$, $^3P_1$, $^1D_2$, and $^1S_0$ of I^+. Also listed are unassigned wavelengths of peaks for I.

A. Wavelengths of features converging to $^3P_0$ of I^+.

1. *ns* series

λ(Å)	$h\nu$(eV)	n^*	Remarks
1186.06	10.4535	4.131	
1155.72	10.7280	5.102	
1140.95	10.8668	5.953	Very weak, ill-defined, uncertain
1129.70	10.9750	7.025	Very weak, ill-defined, uncertain
1102.02	11.2507	∞	

2. *nd* series

λ(Å)	$h\nu$(eV)	n^*	Remarks
1168.63	10.6094	4.606	
1145.95	10.8194	5.617	
1133.03	10.9428	6.647	
1124.73	11.0236	7.739	
1119.25	11.0775	8.863	Shoulder
1102.02	11.2507	∞	

B. Wavelengths of features converging to $^3P_1$ of I^+.

1. *ns* series

λ(Å)	$h\nu$(eV)	n^*	Remarks
1182.76	10.4827	4.008	
1149.45	10.7865	5.004	Very sharp, not very strong
1132.65	10.9465	5.957	Shoulder
1120.65	11.0637	7.149	Weak, but distinct
1115.66–1115.76	11.1132–11.1122	7.924–7.905	Rather big, broad peak
1111.15	11.1583	8.904	Big peak, may be composite
1107.45	11.1956	10.064	
1105.24	11.2179	11.025	Shoulder
1103.81	11.2325	11.818	Big peak
1102.40	11.2468	12.800	Somewhat broader peak than expected
1101.20	11.2591	13.864	
1100.30–1100.40	11.2683–11.2673	14.865–14.743	
1099.48–1099.58	11.2767–11.2757	15.996–15.844	
1098.88–1098.98	11.2829–11.2818	17.012–16.829	
1094.32	11.3299	∞	

2. *nd* series (minima chosen for sequence)

λ(Å)	$h\nu$(eV)	n^*	Remarks
~1160.92	~10.6800	4.575	Broad minimum, very broad maximum nearby
~1138.67	~10.8886	5.553	Same as above, minimum slightly better defined
1125.94	11.0117	6.539	
~1117.47	~11.0952	7.614	
1112.35	11.1462	8.607	
1108.95	11.1804	9.541	
1106.35	11.2067	10.509	
1104.20	11.2285	11.585	
1102.81	11.2427	11.490	
1101.70	11.2540	13.389	Minimum not as pronounced
1100.79	11.2633	14.294	Minimum not as pronounced
1100.00	11.2714	15.250	Minimum not as pronounced
1094.321	11.3299	∞	

TABLE I. (*Continued.*)

C. Wavelengths of features converging to $^1D_2$ of I^+.

1. *ns* series (sharp peaks)

λ(Å)	$h\nu$(eV)	n^*	Remarks
1166.40	10.6297	2.988	
1096.23	11.3101	4.017	
1067.58	11.6137	5.022	
1052.43	11.7808	6.045	
1043.82	11.8780	7.032	
1038.32	11.9409	8.007	Intense
1034.33	11.9870	9.051	
1031.57	12.0190	10.072	
1029.57	12.0424	11.083	
1028.22	12.0582	11.971	Shoulder
1020.19	12.1532	∞	

2. *ns′* series (sharp peaks)

λ(Å)	$h\nu$(eV)	n^*	Remarks
1157.93	10.7075	3.0683	May be doublet
(1157.53)	(10.7112)	(3.072)	
~1091.03	11.3640	4.152	Broad peak, chose highest pt.
1065.53	11.6360	5.129	
1051.34	11.7931	6.147	Reversal of intensity ratio between *ns* and *ns′* series
1043.42	11.8825	7.091	
1037.92	11.9455	8.095	
1020.19	12.1532	∞	

3. *nd* series

λ(Å)	$h\nu$(eV)	n^*	Remarks
1111.45–1111.55	11.1553–11.1543	3.692–3.691	
1074.78	11.5358	4.695	
1057.58	11.7223	5.620	Very sharp - unusual for *nd* series
1047.48	11.8366	6.556	Also very sharp
1040.57	11.9151	7.560	Very sharp, shoulder
1035.87	11.9691	8.599	Very sharp
1032.96	12.0029	9.515	Very sharp
1030.67	12.0295	10.491	Shoulder
1028.87	12.0506	11.520	Shoulder
1020.19	12.1532	∞	

4. *nd′* series

λ(Å)	$h\nu$(eV)	n^*	Remarks
1106.63	11.2038	3.786	
~1072.7	~11.5582	4.782	Very poorly defined
~1055.98	~11.7412	5.747	Not well-defined, broad
1046.37	11.8490	6.689	
1039.37	11.9288	7.788	Noisy, took highest point
1035.23	11.9766	8.779	
1032.53	12.0079	9.679	
1030.47	12.0319	10.591	
1028.57	12.0541	11.722	
1027.53	12.0664	12.522	
1026.52	12.0782	13.469	Poorly defined
1020.19	12.1532	∞	

TABLE I. (*Continued.*)

D. Wavelengths of features converging to $^1S_0$ of I^+.

1. *ns* series ("anomalous profile")

λ(Å)	$h\nu$(eV)	n^*	Remarks
935.29	13.2564	3.995	Peak
~934.58	13.2665	4.019	Minimum
913.56	13.5717	5.032	Minimum
902.46	13.7386	6.061	Minimum
~895.95	~13.8384	7.092	Minimum, poorly defined
878.77	14.1090	∞	

2. *nd* series

λ(Å)	$h\nu$(eV)	n^*
949.87	13.0528	3.589
920.68–920.76	13.4667–13.4656	4.603–4.599
906.55	13.6766	5.610
898.55	13.7983	6.618
878.77	14.1090	∞

E. Unassigned wavelengths of peaks for I.[a]

λ(Å)	$h\nu$(eV)	Remarks
1149.85	10.7827	Weak, sharp
1137.25	10.9022	Doublet, moderate
1136.85	10.9060	Doublet, moderate
1118.75	11.0825	Broad, moderate
1114.86	11.1211	Moderate, sharp
1114.15	11.1282	Moderate, sharp
1113.16	11.1381	Moderate, sharp
1108.24	11.1876	Broad, moderate
1106.65	11.2036	Moderate, sharp
1104.73	11.2231	Moderate, sharp
1077.09	11.5111	Broad, moderate
1073.98	11.5445	Broad, moderate

[a]Features at 1118.75 Å and 1077.09 Å may be early members of another *nd* series converging to $^1D_2$, with effective quantum numbers 3.56 and 4.60. Resolution is insufficient to clearly distinguish higher members.

TABLE II. Electric-dipole-allowed Rydberg excitations of Te.

Initial state	Ionic core	Rydberg l_j	Total J of allowed final state
Te: $p^4, {}^3P_2$	$p^3, {}^2P_{1/2}$	$s_{1/2}$	1
		$d_{3/2}$	1,2
		$d_{5/2}$	2,3
	$p^3, {}^4S_{3/2}$	$s_{1/2}$	1,2
	$p^3, {}^2P_{3/2}$	$d_{3/2}$	1,2,3
	$p^3, {}^2D_{3/2}$	$d_{5/2}$	1,2,3
	$p^3, {}^2D_{5/2}$	$s_{1/2}$	2,3
		$d_{3/2}$	1,2,3
		$d_{5/2}$	1,2,3

limit corresponding to the process

$$(5s)^2(5p)^4 + h\nu \rightarrow 5s(5p)^4({}^4P_{5/2}) + e\,. \qquad (1)$$

The window resonances occur at ~795, 741, and 722 Å, corresponding to $n^* = 2.463$, 3.518, and 4.519, respectively, and appear similar to inner *s* electron excitations in the heavier noble gases. The limit of this series (λ = 695.12 Å) can be obtained from Moore.[19]

Very sparse information exists in the literature regarding Rydberg series converging to the limit of Eq. (1). Morillon and Vergés[20] have interpreted some of the lines reported earlier by McLennan[21] in emission spectra as evidence for a $5s5p^5$ configuration, with $^3P_2$ at 63 296.823 cm^{-1} (1579.858 Å) and $^3P_1$ at 64 308.139 cm^{-1} (1555.013 Å) above the ground state. Both of these energies fall below the first ionization potential and hence are outside our

experimental range. They correspond to effective quantum numbers $n^*=1.167$ and 1.174, respectively. The quantum defects for these states are substantially different from those observed in the window-resonance series.

Cheng and Kim[22] have performed multiconfiguration Dirac-Fock (MCDF) calculations on TeI to determine the energy levels of $5s5p^5$ and $5s5p^4np$ ($n=6,7,8$) for the $J=1$, 2, and 3 sequences and the oscillator strengths for the corresponding transitions from the $^3P_2$ ground state. The $5s5p^5$ configuration cannot have $J=3$. The $5s5p^4np$ configurations have seven $J=3$ components. Of these, five converge to higher limits than that given in Eq. (1). Of the remaining two, one has oscillator strength $\sim 10^{-2}$, the other $\sim 10^{-4}$. The effective quantum numbers for the series with larger oscillator strengths are $n^*=2.564$, 3.599, and 4.610 for $n=6$, 7, and 8, respectively. These values of n^* match fairly well with the effective quantum numbers of our window-resonance series. A further argument for this assignment is the absence of an $n=5$ member in the window-resonance series.

By contrast, the $5s5p^5$ configuration yields two $J=1$ and one $J=2$ states. The oscillator strengths to these states are larger by one to two orders of magnitude than to any of the other states calculated by Cheng and Kim. The computed effective quantum numbers for the $J=1$ state are 1.448 and 2.438, with oscillator strengths of ~5 and 0.5. For the $J=2$ state, they calculate $n^*=1.403$, with an oscillator strength ~10.

The most intense feature in Fig. 2 by far occurs at about 1038.4 Å, which corresponds to $n^*=1.519$ for the limit given by Eq. (1). The next most intense feature, at about 1060.5 Å, corresponds to $n^*=1.488$. Both the intensities and effective quantum numbers of these two features are in fair agreement with the calculated values of Cheng and Kim for $5s5p^5$, $J=1$ and 2. The positions of these levels inferred by Morillon and Vergés are at much lower effective quantum numbers. Furthermore, although the $5s5p^5$ configuration can be expected to have a larger interaction with the core than the higher members ($5s5p^4np$), we shall see that our assignments for $5s5p^5$ have quantum defects more in line with the higher members than those given by Morillon and Vergés.

We have already considered the higher members of the $J=3$ sequence. For $5s5p^4np$, Cheng and Kim find fourteen $J=1$ states and thirteen $J=2$ states. Of these, all but two in the $J=2$ sequence (and probably also in the $J=1$ sequence) converge to limits higher than that in Eq. (1). Of the remaining two, one has an oscillator strength about an order of magnitude larger than the other. The more intense $5s5p^46p$ component has a computed $n^*=2.584$ for $J=1$ and $n^*=2.835$ for $J=2$. In Fig. 2 we can identify two peak-type features at 788.79 and 777.69 Å, having $n^*=2.534$ and 2.680 corresponding to the limit of Eq. (1). Normalized to the most intense peaks in the spectrum, these features are about one order of magnitude more intense than the relative oscillator strengths for these $n=6$ components calculated by Cheng and Kim. Therefore, we tentatively assign the lower n^* component to $J=1$, and the higher one to $J=2$ of the $n=6$ configuration. There is evidence in the spectrum for $n=7$ and $n=8$ members of these series.

In summary, the calculations of Cheng and Kim provide a basis for relating the most intense peaks in the tellurium spectrum to the window resonances, both of which involve excitation of the inner 5s orbital. In both calculation and experiment, there is a drastic diminution in oscillator strength between $5s5p^5$ and $5s5p^46p$ for the $J=1$ and $J=2$ sequences.

The arguments presented above have led us to assign the window resonances ($q\approx 0$) to $J=3$ states and the peaks ($|q|\gg 0$) to $J=1$ and $J=2$ states. We have tried to examine reasons for this drastic disparity in the shape of the resonance states. Depending upon the nature of the outgoing wave (s or d), the continua can have either $J=1$, 2, or 3 character and therefore can interact with each of the resonant states. The shape profile index q is defined by Fano[17] as

$$q=\frac{M}{\pi Vm},$$

where M is the transition moment connecting ground state and quasidiscrete state, m is the moment connecting ground state and continuum in the same energy range, and V is the configuration interaction between discrete state and continuum. The oscillator-strength calculations for the $n=6$, 7, and 8 regions yield results of similar magnitude for $J=1$, 2, and 3, which tends to rule out the numerator as a controlling factor in the magnitude of q. At this point we are unable to distinguish between the relative importance of V or m in determining the value of q. The valley of the window resonance reduces the continuum by 0.3. A recent photoelectron spectrum of tellurium obtained in our laboratory[23] indicates roughly equal intensities of $^4S_{3/2}$, $^2D_{3/2}$, and $^2D_{5/2}$ states of Te^+, with negligible intensities of $^2P_{1/2}$ and $^2P_{3/2}$. This evidence suggests that just one of the three major ionization continua is interacting with the $J=3$ resonances. For this interaction to occur, the continuum must also have $J=3$ character. If

the departing electron corresponding to each of the major continua was of s character, then only the $^2D_{5/2}$ component could form a $J=3$ continuum. If the departing electron had a significant d-wave component in each of the continua, then they each could acquire $J=3$ character and an assessment of the diminution in the continuum would require detailed knowledge of the wave functions.

The wavelengths of identified features in these series, together with their effective quantum numbers, are listed in Table III. Unidentified lines are given in a subset of this table.

TABLE III. Wavelengths of identified features in Rydberg series, converging to $5s^2\,5p^3\,^2D_{3/2}$, $^2D_{5/2}$, $^2P_{1/2}$, $^2P_{3/2}$, and $5s5p^4(^4P_{5/2})$ of Te^+. Also listed are unassigned wavelengths of peaks for Te.

A. Wavelengths of features converging to $^2D_{3/2}$ of Te^+.

1. ns series

λ(Å)	$h\nu$(eV)	n^*	Remarks
1308.92	9.4723	4.112	
1267.78	9.7797	5.230	
1251.43	9.9075	6.067	
1237.76	10.0169	7.231	Coincident with big peak converging to $^2P_{3/2}$
1231.91	10.0645	7.999	Coincident with big peak converging to $^2P_{3/2}$
1225.62	10.1161	9.193	
1221.61	10.1493	10.318	
1219.42	10.1676	11.144	
1217.62	10.1826	11.997	Coincident with 2 other series
1216.27	10.1939	12.786	Merged with nd' series
1214.76	10.2066	13.886	Merged with nd' series
1213.67	10.2157	14.887	Merged with nd' series
1212.81	10.2230	15.852	Merged with nd' series
1206.42	10.2771	∞	

2. nd series

λ(Å)	$h\nu$(eV)	n^*	Remarks
1342.98	9.2321	3.608	
1284.97	9.6489	4.654	Weak and ill defined
1259.58	9.8434	5.601	Highest point chosen
1244.51	9.9626	6.577	Highest point chosen
1235.36	10.0364	7.518	Highest point chosen
1228.22	10.0947	8.636	Highest point chosen
1224.11	10.1286	9.571	Highest point chosen Large peak—must be composite
1206.42	10.2771	∞	

3. nd' series

λ(Å)	$h\nu$(eV)	n^*	Remarks
1339.48	9.2562	3.651	Highest point chosen
1281.08	9.6782	4.766	Highest point chosen May be split peak with other maximum at 1281.64 Å
~1258.40	9.8526	5.661	May be 2 peaks separated by 0.25 Å; midpoint chosen
1242.36	9.9798	6.765	Surprisingly large peak
1234.26	10.0453	7.661	
1227.52	10.1005	8.776	Highest point chosen; 2 other high points at 1227.42 and 1227.32 Å
1223.56	10.1332	9.725	Shoulder
1220.52	10.1584	10.705	
1218.02	10.1792	11.797	Shoulder
1206.42	10.2771	∞	

TABLE III. (*Continued.*)

B. Wavelengths of features converging to $^2D_{5/2}$ of Te^+.

1. *ns* series

λ(Å)	$h\nu$(eV)	n^*	Remarks
1367.92	9.0638	3.026	
1275.47	9.7208	4.051	
1237.76	10.0169	5.053	Coincident with $^2P_{3/2}$ series and $^2D_{3/2}$, *ns* series
1217.62	10.1826	6.087	Coincident with $^2D_{3/2}$, *ns* and *nd'* series
1206.27	10.2784	7.081	
1199.12	10.3397	8.047	
1194.48	10.3798	8.948	
1190.23	10.4169	10.119	
1187.58	10.4402	11.141	
1185.83	10.4556	12.017	
1184.38	10.4684	12.928	Merged with $^2D_{5/2}$, *nd* series
1183.13	10.4794	13.906	Merged with $^2D_{5/2}$, *nd* series
1182.13	10.4883	14.875	Merged with $^2D_{5/2}$, *nd* series
1175.24	10.5498	∞	

2. *nd* series

λ(Å)	$h\nu$(eV)	n^*	Remarks
~1294.33	9.5791	3.744	Middle of broad peak
~1247.80	9.9363	4.709	Shoulder in broad complex
~1223.11	10.1369	5.740	Peak
~1209.62	10.2474	6.708	Broad shoulder
1200.47–1200.68	10.3280–10.3262	7.834–7.802	2 data sets differ slightly in peak maximum
1195.27–1195.33	10.3730–10.3725	8.773–8.760	2 data sets differ slightly in peak maximum
1191.43	10.4064	9.742	
1175.24	10.5498	∞	

C. Wavelengths of features converging to $^2P_{1/2}$ of Te^+.

nd series

λ(Å)	$h\nu$(eV)	n^*	Remarks
1287.68	9.6286	2.656	
1177.05	10.5336	3.646	Very weak evidence for peak
1135.80	10.9161	4.607	Weak
1114.85	11.1212	5.587	Weak
1102.00	11.2509	6.666	Weak
1072.80	11.5572	∞	

D. Wavelengths of features converging to $^2P_{3/2}$ of Te^+.

1. *ns* series

λ(Å)	$h\nu$(eV)	n^*	Remarks
1180.91	10.4991	3.022	
1112.10	11.1488	4.024	
1082.43	11.4543	5.044	
1034.14	11.9892	∞	

2. *nd* series

λ(Å)	$h\nu$(eV)	n^*	Remarks
1237.79	10.0167	2.626	Coincident with $^2D_{3/2}$, *ns* series
1131.15	10.9610	3.638	
1034.14	11.9892	∞	

TABLE III. (*Continued.*)

D. Wavelengths of features converging to $^2P_{3/2}$ of Te^+.

3. nd' series

λ(Å)	$h\nu$(eV)	n^*	Remarks
1231.94	10.0642	2.659	Coincident with $^2D_{3/2}$, ns series
~1128.00	10.9916	3.693	
~1090.30	11.3717	4.694	
1071.48	11.5714	5.706	
~1061.12	11.6844	6.681	Shoulder on big peak
1034.14	11.9892		

E. Wavelengths of features converging to $5s5p^4$ ($^4P_{5/2}$) of Te^+.

1. np ($q \simeq 0$) series ($J=3$)

λ(Å)	$h\nu$(eV)	n^*	Remarks
~795.10	15.5938	2.463	Some uncertainty in establishing precise minimum
~740.79	16.7369	3.518	Some uncertainty in establishing precise minimum
~722.09	17.1704	4.519	Minimum better defined here
695.12	17.8365	∞	

2. np' series (maxima)

λ(Å)	$h\nu$(eV)	n^*	Remarks
1060.46	11.6916	1.488	$5s5p^5$, probably $J=1$
1038.44	11.9396	1.519	$5s5p^5$, probably $J=2$
788.79	15.7184	2.534	$5s5p^46p$, probably $J=1$
777.69	15.9428	2.680	$5s5p^46p$, probably $J=2$
739.89–739.99	16.7573–16.7551	3.551–3.547	
721.39–721.49	17.1871–17.1847	4.577–4.569	
695.12	17.8365		

F. Unassigned wavelengths of peaks for Te

λ(Å)	$h\nu$(eV)	Remarks
~1360.77	9.1114	Broad
~1320.62	9.3884	Broad, weak
~1290.45	9.6079	Broad, weak
1278.88	9.6948	Broad, moderate
1212.01	10.2297	Sharp, moderate
1053.67	11.7670	Intense
1051.56	11.7906	Intense
1043.57	11.8809	Intense, sharp
1042.66	11.8912	Intense, sharp
1041.52	11.9042	Intense
1040.72	11.9134	Moderate

IV. DISCUSSION AND CONCLUSIONS

The photoionization yield curve of atomic iodine has been measured from ~645 Å to the ionization threshold. We have observed most of the features that appeared in the photographic absorption work of Huffman *et al.*[24] Many, but not all of the allowed Rydberg series can be seen. Those series identified as Rydberg d like have quantum defects of ~0.4 (modulo 1), $q \approx 1$ and are relatively intense. Others identified as Rydberg s-like series have quantum defects of ~0 and are sharp peaks. We have verified the higher ionization energy for $^1S_0$ given by Huffman *et al.*, which differs significantly from the value given in Moore's tables.

The photoionization-yield curve of tellurium has some similarities to that of iodine (and indeed, that of xenon[25]) in that the Rydberg d-like excita-

tions are relatively intense and have quantum defects of ~0.4 and $q \approx 1$. The inner 5*s* orbital excitations have been observed, and display window resonances similar to those in the noble gases. When account is taken of the difference in excitation energies between initial $^3P_2$ and $^1S_0$ states, no visible correlation is seen between our autoionization pattern for Te and that calculated by McGuire.[13] McGuire's calculations led him to question the ionization energy given by Moore, but the present results are in good agreement with all of Moore's ionic energies encompassed by our data.

Finally, we shall try to make some comparisons between the present results on iodine and the two calculations that have incorporated resonance features on the related chlorine atom. Both the *R*-matrix[11] and many-body perturbation-theory[12] calculations deduce a strong Rydberg *d*-like series converging to $^1D_2$ and having an anomalous resonance profile. Lamoureux and Combet-Farnoux[11] calculate $q \simeq 3.6$ for this resonance, probably somewhat higher than the value we would estimate for iodine, but generally a similar shape with minimum preceding maximum. Also comparable is one series of resonances converging to $^1S_0$. This one series consists of peaks superposed upon continuum (relatively high q) and is obtained in both calculations. The *R*-matrix calculations display a much larger peak to continuum ratio than do the many-body perturbation-theory results. The iodine data look rather like the latter. Brown *et al.*[12] also calculate window-resonance features for the inner *s* excitations of chlorine. While we have not observed these for iodine, we do see them in tellurium. Hence, despite the complexities introduced by the many series that become allowed with open-shell atoms, some patterns have begun to emerge.

ACKNOWLEDGMENTS

We wish to thank Dr. R. E. Huffman for sending us photographic reproductions of his iodine absorption spectra, together with assignments, which are as yet unpublished. We should also like to thank Dr. K.-T. Cheng and Dr. Y.-K. Kim for performing the multiconfiguration Dirac-Fock calculations on tellurium which provided strong evidence for our assignment of experimental features to the $5s5p^4np$ configuration, and provided additional details regarding the J values of these states. Our research was performed under the auspices of the Division of Basic Energy Sciences of the United States Department of Energy.

[1] S. T. Manson, Adv. Electron. Electron Phys. 41, 73 (1976); 44, 1 (1977).
[2] M. Ya. Amusia and N. A. Cherepkov, Case Stud. At. Phys. 5, 47 (1975); N. A. Cherepkov and L. V. Chernysheva, Phys. Lett. 60A, 103 (1977).
[3] H. P. Kelly, Adv. Theor. Phys. 2, 75 (1968); Adv. Chem. Phys. 14, 129 (1969); S. L. Carter and H. P. Kelly, Phys. Rev. A 13, 1388 (1976).
[4] P. G. Burke and W. D. Robb, in *Advances in Atomic and Molecular Physics*, edited by D. R. Bates and B. Bederson (Academic, New York and London, 1975), Vol. 11, p. 143.
[5] W. R. Johnson, K. T. Cheng, K.-N. Huang, and M. LeDourneuf, Phys. Rev. A 22, 989 (1980).
[6] P. Shorer and A. Dalgarno, Phys. Scr. 21, 432 (1980).
[7] J.-J. Chang, J. Phys. B 10, 3195 (1977).
[8] S. T. Manson, A. Msezane, A. F. Starace, and S. Shahabi, Phys. Rev. A 20, 1005 (1979).
[9] K. Kimura, T. Yamazaki, and Y. Achiba, Chem. Phys. Lett. 58, 104 (1978).
[10] J. Berkowitz and G. L. Goodman, J. Chem. Phys. 71, 1754 (1979).
[11] M. Lamoureux and F. Combet-Farnoux, J. Phys. (Paris) 40, 545 (1979).
[12] E. R. Brown, S. L. Carter, and H. P. Kelly, Phys. Rev. A 21, 1237 (1980); Phys. Lett. 66A, 290 (1978).
[13] E. J. McGuire, Phys. Rev. A 19, 1978 (1979).
[14] J. Berkowitz, C. H. Batson, and G. L. Goodman, J. Chem. Phys. 71, 2624 (1979).
[15] E. Schubert and R. D. Hudson, *A Photoelectric Atlas of the Intense Lines of the Hydrogen Molecular Emission Spectrum from 1025 to 1650 Å at a Resolution of 0.10 Å*, Defense Technical Information Center Technical Report No. 422867, Aerospace Corp. Report No. ATN-64 (9233)-2 (1963).
[16] R. E. Huffman, J. C. Larrabee, and Y. Tanaka, J. Chem. Phys. 47, 856 (1967); 48, 3835 (1968).
[17] U. Fano, Phys. Rev. 124, 1866 (1961).
[18] K. B. S. Erikkson, J. Opt. Soc. Am. 64, 1272 (1974).
[19] C. E. Moore, *Atomic Energy Levels*, U. S. N. B. S. Circular No. 467 (U. S. Government Printing Office, Washington, D. C., 1958), Vol. III.
[20] C. Morillon and J. Vergès, Phys. Scr. 12, 129 (1975).
[21] J. C. McLennan and M. F. Crawford, Nature 124, 874 (1929).
[22] K.-T. Cheng and Y.-K. Kim, unpublished results, private communication.
[23] G. L. Goodman and J. Berkowitz (unpublished).
[24] R. E. Huffman has kindly provided us with photographic absorption spectra and wavelengths of lines observed in his iodine studies, which are as yet unpublished.
[25] For quantum defects in noble gases, see K. Radler and J. Berkowitz, J. Chem. Phys. 70, 216 (1979). For corresponding values of the profile index q, see K. Radler and J. Berkowitz, J. Chem. Phys. 70, 221 (1979). The photoionization yield curve of xenon appears in J. Berkowitz, *Photoabsorption, Photoionization and Photoelectron Spectroscopy* (Academic, New York, 1979), p. 181.